Experimental and Self-Consistent-Field Theoretical Study of Styrene Block Copolymer Self-Adhesive Materials

Kostas Ch. Daoulas[†] and Doros N. Theodorou*[,‡]

Institute of Chemical Engineering and High-Temperature Chemical Processes, ICE/HT-FORTH, GR 26500, Patras, Greece, and School of Chemical Engineering, Department of Materials Science and Engineering, National Technical University of Athens, 9 Heroon Polytechniou Street, Zografou Campus, 15780 Athens, Greece

Alexandra Roos[§] and Costantino Creton

École Supérieure de Physique et Chimie Industrielles, Laboratoire PCSM, Bâtiment H, 10 rue Vauquelin, 75231 Paris, Cedex 05, France

Received September 16, 2003; Revised Manuscript Received March 29, 2004

ABSTRACT: This work addresses thermodynamic and mechanical properties of styrene block copolymer (SBC) self-adhesive materials. Mixtures of polystyrene-*block*-polyisoprene-*block*-polystyrene (SIS triblock) copolymers with resin and their blends with polystyrene-*block*-polyisoprene (SI diblock) copolymers were investigated experimentally and theoretically. The experiments involved small-angle X-ray scattering, atomic force microscopy, and tensile measurements, while the theoretical analysis invoked a mesoscopic representation of SBC materials combined with a continuum, 3D real-space self-consistent-field (SCF) approach. The calculations predict that the SBC systems should become microphase separated, with PS-rich spherical domains forming a bcc lattice in SIS triblock/SI diblock blends and in SIS triblock/resin systems with low resin content (20 wt %), while at high (60 wt %) resin content a disordered structure of PS-rich domains is expected. Extensive comparisons of SCF predictions concerning the type and the geometric characteristics of the morphologies obtained, the composition profiles, and the effect of diblock and resin content on the long-range space ordering of the PS-rich domains are performed against the experimental data. SCF theory predicts that approximately 79% of SIS molecules are connecting different PS-rich domains (i.e., are forming bridges) in SIS/SI blends, almost independently of the SI diblock content. The SCF results are combined with a slip tube model of rubber elasticity to predict the elastic behavior of SBC materials. In particular, the bridging properties are used to estimate the PS-rich domain cross-linking contribution, G_c, to the total shear modulus. The entanglement contribution, G_e, is evaluated from experimental and theoretical results reported in the literature concerning the properties of entanglements. The predicted stress−strain curves are in good qualitative agreement with the tensile experimental data for small values of strain.

1. Introduction

Pressure-sensitive adhesive (PSA) materials are extensively utilized in everyday life in the form of self-adhesive tapes, labels, and tags as well as in more specialized technological and medical applications.[1,2] Very briefly, they can be described as consisting mainly of two types of components: polymer, accounting for the overall strength, and tackifiers, providing adhesion and controlling the viscosity of the system during industrial processing. Styrenic block copolymer (SBC) based adhesives constitute a special case of these systems and are particularly interesting due to their excellent adhesive strength, which is especially important in applications where long-term resistance to moderate levels of shear stresses is required. They have the additional advantage of being produced by the environmentally friendly hot-melt technology. However, they suffer from two important limitations: low maximum temperature of use and inferior aging resistance in comparison to the acrylic PSA materials, which are typically based on statistical copolymers. To improve the performance of styrenic block copolymer PSA's in relation to these properties, it is necessary to understand the reasons for the high strength of block copolymer based adhesives and to exploit this understanding in designing equivalent systems with better aging and temperature resistance. SBC based adhesives are generally blends of styrene−isoprene−styrene triblock copolymers and styrene−isoprene diblock copolymers compounded with a low molecular weight but high-T_g resin based on C5 rings, which is miscible with the isoprene phase but immiscible with the styrene phase. It is important to note that the tackifying resin is a necessary component for this class of PSA in order to obtain PSA properties.[3−5]

To obtain usable PSA properties, the proportion of styrene in the compounded PSA must be of the order of 4−12%, the molecular weight of the styrene block must be above 10−11 kg/mol to stay immiscible with the isoprene phase, and the weight fraction of polymer in the blend typically varies[2] between 25 and 45%. Because of the use of mutually immiscible blocks, these PSA's are really nanophase separated, with styrene domains dispersed in an isoprene matrix. It is believed that these styrene domains provide physical cross-links, which give

[†] ICE/HT-FORTH.
[‡] National Technical University of Athens.
[§] Current address: Essilor International, Recherche et Développement Matériaux, Lens Material and Technology, 57, avenue de Condé, St-Maur-des-Fossés Cédex 94106, France.
* To whom correspondence should be addressed: Tel (+30) 210 772 3157; Fax: (+30) 210 772 3112; e-mail doros@central.ntua.gr.

10.1021/ma035383a CCC: $27.50
Published on Web 05/25/2004

Table 1. Experimentally Obtained Characteristics of the SBC Systems Studied in the Present Work[a]

sample code	β_{SIS}	β_{SI}	β_R	MW resin (kg/mol)	MW SI (kg/mol)	α_{SI}	MW SIS (kg/mol)	α_{SIS}
T2	1						154	0.151
T2D19	0.81	0.19			72	0.15	154	0.151
T2D42	0.58	0.42			72	0.15	154	0.151
T3D54	0.46	0.54			72	0.16	176	0.161
T2R20	0.80		0.20	0.370			154	0.151
T2R40	0.60		0.40	0.370			154	0.151
T2R60	0.40		0.60	0.370			154	0.151

[a] α_{SI} and α_{SIS} are the weight fractions of styrene in the SI and SIS copolymer molecules, respectively. β_{SIS}, β_{SI}, and β_R are the weight fractions of SIS, SI, and resin in the copolymer/resin mixture.

these PSA's a superior resistance to creep. Not all physically cross-linked polymers display such interesting properties, however, and the details of how the network of physical cross-links are organized and can be deformed remain largely unknown.

The present work is aimed to contribute in this direction in two ways: (a) by exploring the structure and the properties of SBC's through various experimental techniques—small-angle X-ray scattering (SAXS), atomic force microscopy (AFM) and tensile tests—and (b) by modeling these materials through field theoretic methods.

The history of implementation of field theoretic methods in block copolymer systems is nearly 3 decades long, starting from the works of Helfand and coworkers.[6−10] Nowadays, the development of computer technology and computational methods for the numerical treatment of the field theory formalism[11−13] has considerably broadened its applications and has actually given rise to a new class of soft condensed matter simulation techniques: the field theoretic simulation methods. As was extensively discussed in Fredrickson et al.,[14] this approach is based on the development of a suitable coarse-grained molecular model for the polymeric system and its subsequent conversion to a field theory. This conversion is carried out through formally exact methods so, at this stage, apart from the initial assumptions invoked in the molecular model construction, no approximation is made. A numerical procedure is then implemented, usually based on proper discretization of the simulation domain in order to sample the "configuration" space of the complex fields entering the field theory formulation. An especially popular type of field theory is the self-consistent field (SCF), which avoids sampling of the field configurational space by introducing a saddle point approximation to the statistical sum of the initial field theory. In this way only a single "configuration" of fields has to be determined: the one with the maximum statistical weight, which is defined through a system of equations. These equations are then solved by implementing a suitable numerical method.[11,15,16]

Further developments[13] in field theoretic methods have also been promising in making them competitive for tracking the long-time dynamic evolution of complex fluid systems, which traditionally were explored only by means of "classic" computer simulation techniques (e.g., molecular dynamics). These methods have been implemented in commercial packages, such as Mesodyn,[16] or in the computer simulation software for multiscale modeling of condensed soft matter systems.[17]

With this background, our modeling objectives are twofold. The first, of a more general character, is to develop a tool capable of generating equilibrium states of styrene block copolymer (SBC) adhesive systems in the framework of mean-field representation. This information could then be incorporated in an entanglement network-based coarse-grained kinetic Monte Carlo approach[18−20] for the simulation of the viscoelastic properties of these materials. The second aim, which is the focus of this paper, is to predict various characteristics of SBC systems at an equilibrium state and to perform detailed comparisons of these results with experimental SAXS, AFM, and mechanical property data. These include comparisons of predictions concerning the type of morphologies developed in SBC systems and their typical length scales against experimental AFM images and SAXS patterns. In addition, conformational properties of block copolymer molecules and information on bridging between domains are derived and used to interpret experimental tensile tests in the light of a recently developed rubber elasticity theory.[21]

2. Experimental Section

The block copolymers were provided by ExxonMobil Chemical, and their molecular characteristics are summarized in Table 1. The tackifying resin was a hydrogenated C5 based resin produced by ExxonMobil Chemical under the trade name Escorez 5380, and its characteristics are also given in Table 1.

To characterize the nanostructure of the SBC based systems, we performed small-angle X-ray scattering measurements (SAXS) and atomic force microscopy scans (AFM) on our model blends.

For the SAXS, we used a Rigaku rotating anode source that produced the Cu Kα lines (1.54 Å) with a fine focus (1 mm × 0.1 mm). The output was collimated by a gold-plated quartz mirror. A nickel plate was placed at the output in order to eliminate the Kβ line. The detector was a linear detector with 512 channels (99 channels/cm) and was placed 81 cm from the sample position. The resolution of the direct beam was measured to be $\Delta q = 0.003$ Å^{-1} full width at half-maximum. In these experiments the collimation corrections are negligible. The samples were ~1 mm thick. To subtract the background, we measured the scattering without any sample during 1 h and subtracted it from the signal of the samples which were also acquired during 1 h.

With these measurements we obtained an estimate of the size of the styrene domains and the average distance between them as a function of the composition. Finally, atomic force microscopy (AFM) experiments were realized using a commercial atomic force microscope (Digital Instrument, Nanoscope IIIa) in tapping mode. Phase was detected using a homemade electronic setup, which included a lock-in amplifier. Regular diving-board-shaped silicon cantilevers were used (NanoProbe, Digital Instruments). Their resonance frequency was about 300 kHz.

We performed AFM phase imaging in order to investigate the nanostructure of SBC based systems at their surface. At room temperature, the styrene domains are glassy and the isoprene is elastomeric and dissipative. In phase imaging, the phase lag of the cantilever oscillation, relative to the signal sent to the cantilever's piezo driver, is very sensitive

to variations in material properties such as adhesion and viscoelasticity.

We performed our tensile tests on a standard tensile testing machine (JFC TC3). The adhesive films were prepared from 14.75 wt % solutions in toluene cast in Teflon molds for the adhesive formulations or in aluminum pans. They were dried 10 days at room temperature and 48 h at 45 °C under vacuum. The samples tested were rectangular with the following dimensions: 300 μm thick, 4 mm wide and 15 mm high (length between the clamps).

Indeed, the rectangular shape was preferred to the classical "dog-bone" shape for its simplicity. In addition, this geometry was found to be more adapted for such soft materials as pressure-sensitive adhesives.[22] The samples being very soft and very adhesive were removed from their Teflon mold by freezing them in liquid nitrogen. They were then placed between two sheets of release paper. The films were cut with scissors at the chosen dimensions and placed in the upper clamp after being frozen in liquid nitrogen; the upper clamp being a simple clip, the sample had to be rigid enough to be fixed.

The tests were then performed at a constant crosshead velocity of 500 mm min^{-1}. They were repeated twice. The force F and displacement L data were directly obtained from the displacement of the crosshead. The nominal stress σ_N and the deformation ϵ data were then calculated using the initial values of the width w_0, the thickness e_0, and the height L_0 of the sample.

The force−displacement curves obtained from the tensile tests were transformed into nominal stress−deformation curves and were then analyzed in terms of reduced stress using the Mooney−Rivlin representation.

3. SCF Theory and Mesoscopic Representation of SBC Systems

The description of a polymeric system in the framework of a SCF approach is intimately linked with the coarse-grained model used to represent the connectivity of polymer molecules and the nonbonded interactions. In this context, a crucial question to be answered is what properties of the polymeric systems should be preserved during the passage from the atomistic to the mesoscopic scale. In the works of Helfand and co-workers,[8,23] this point is very clearly addressed through the statement that, although the mesoscopic representation of the polymeric system is not unique, some quantities, called invariants, must be preserved on a mesoscopic scale. The values of these quantities are set by the experimentally established data, characterizing the real polymer systems.

It is now understood[18,24] that a correct mesoscopic model should preserve the density, chain contour length, and chain gyration radius of the real polymer. In a lattice-based SCF approach this requirement can be satisfied by introducing a mesoscopic bending potential in the well-known formalism of Scheutjens and Fleer,[25] while in a continuous space SCF theory, this can be achieved by using more sophisticated models than the classical Gaussian model for chain connectivity.[26−28] However, the present work is aimed at a rather semiquantitative understanding of properties of the SBC systems; thus, we will adopt the Gaussian chain connectivity representation following closely the method of mapping suggested by Helfand[8,23] and co-workers, although it has the disadvantage to preserve, from all the characteristic length scales of the real polymer chain, only the gyration radius.

Assuming that all species mix with no change of volume, we will define the quantities considered as invariants in this work. These will be all the characteristic macroscopic volumes, namely the total volume V and the volumes V^S, V^I, and V^R that would be occupied by each of three components: styrene, isoprene, and resin, respectively, if they constituted pure bulk phases. For the case of blends of diblocks and triblocks we will need four additional volume parameters: the volumes V^S_{SIS}, V^I_{SIS}, V^S_{SI}, and V^I_{SI} occupied by the "triblock" styrene, the "triblock" isoprene, the "diblock" styrene, and the "diblock" isoprene, respectively, should be preserved during the coarse-graining procedure. The next group of invariants are the numbers of molecules n_{SIS}, n_{SI}, and n_R of each different species (triblock, diblock, and resin) present in the system. In our approach the polymerization degree of the mesoscopic chains generally differs from that of the real polymer molecules, so the number densities of the various system components depend on the choice of the mesoscopic representation.[8] To this end, for describing the spatial distribution of the system components independently of the mesoscopic representation, the reduced number densities (volume fractions) will be introduced:

$$\varphi_A(\mathbf{r}) = \rho_A(\mathbf{r})/\rho_{A0} \tag{1}$$

In eq 1, index A denotes the component styrene (S), isoprene (I), or resin (R), while $\rho_A(\mathbf{r})$ and ρ_{A0} stand for the mesoscopic number density of component A in the mixture and in the pure phase, respectively. The squared gyration radii of the polystyrene and the polyisoprene blocks in SIS and SI molecules should also be preserved on the mesoscopic level and will be denoted as R^2_{gS}(SIS), R^2_{gI}(SIS), R^2_{gS}(SI), and R^2_{gI}(SI). Their evaluation is carried out through

$$R^2_{gS} = \frac{1}{6} C^S_\infty 2 n^S_{mer} l^2_{(S)ave}, \quad R^2_{gI} = \frac{1}{6} C^I_\infty 4 n^I_{mer} l^2_{(I)ave} \tag{2}$$

where n^S_{mer} and n^I_{mer}, $l^2_{(S)ave}$ and $l^2_{(I)ave}$, and C^S_∞ and C^I_∞ are the numbers of (chemical) repeat units, the average square skeletal bond lengths, and the characteristic ratios for the polystyrene and the polyisoprene, respectively.

In this work we will follow a common practice adopted in block copolymer melts and solutions[11,14,29] of describing the nonbonded interactions $U_{AB}(\mathbf{r})$ between species A and B in the framework of Flory−Huggins theory:

$$U_{AB} = \chi_{AB}\rho_0 \int_V \varphi_A(\mathbf{r})\, \varphi_B(\mathbf{r})\, d\mathbf{r} \tag{3}$$

where χ_{AB} is the Flory−Huggins interaction parameter of the A and B component pair, while ρ_0 expresses an average number density of the system. It can be seen that the final class of parameters required is a set of invariants, expressed by the products $\chi_{AB}\rho_0$, measuring the strength of nonbonded interactions between the different components of the system. The physical meaning of keeping $\chi_{AB}\rho_0$ invariant is that the mesoscopic and the real system must have the same cohesive energy per unit volume. They can be evaluated either from the Hildebrand solubility parameters, δ_A and δ_B, overlooking any possible entropic contribution to the χ_{AB}:

$$\chi_{AB}\rho_0 = \frac{(\delta_A - \delta_B)^2}{k_B T} \tag{4}$$

or from experimentally established equations, such as

the Rounds and McIntire formula for the case of styrene−isoprene monomer interaction:[30]

$$\chi_{SI}\rho_0 = \left(-900 + \frac{7.5 \times 10^5}{T}\right) \text{mol/m}^3 \qquad (5)$$

with T being the absolute temperature in K.

After defining the invariant quantities, it is possible to proceed to a parametrization suitable for the development of a SCF theory. For convenience, it can be carried out in terms of quantities that are not conserved during the coarse-graining procedure. This does not violate the concept of invariants, as long as the final results of the analysis depend only on combinations of invariant quantities. In all cases of SBC's modeled here, the SIS molecules are symmetric: the two PS end-blocks are identical. In SIS melts we will consider a system of n_{SIS} molecules, occupying a volume V. The polymerization degree of mesoscopic SIS chains and of each of the two PS blocks will be N_{SIS} and N^S_{SIS}, respectively, while the asymmetry parameter $2f_{SIS} = 2N^S_{SIS}/N_{SIS}$ defines the fraction of styrene segments per SIS chain. For convenience, we also introduce a symbol for the degree of polymerization of the PI middle block: $N^I_{SIS} = N_{SIS} - 2N^S_{SIS}$. In the SIS/SI blends, apart from the triblock chains, n_{SI} diblock molecules are also present with a total polymerization degree N_{SI}. The symbols N^S_{SI} and N^I_{SI} denote in this case the polymerization degrees of the PS and the PI blocks of the diblock, respectively, while the asymmetry parameter $f_{SI} = N^S_{SI}/N_{SI}$ defines the fraction of styrene segments per SI chain. The notation used for the description of SIS/resin solutions is similar to the SIS melt, with the exception that we also have to account for the n_R resin molecules.

We will now choose to work in a specific mesoscopic representation, where the number densities of styrene, isoprene, and resin components in the pure phase are equal to each other. In the SIS/SI blends we will separately account for the densities of the styrene and the isoprene in dependence on whether they belong to the SIS or the SI chains, by setting them explicitly equal to each other. This general conversion for the density can be summarized as follows:

(a) For the SIS/SI blends:

$$\frac{N_{SIS}n_{SIS}}{V_{SIS}} = \frac{N_{SI}n_{SI}}{V_{SI}} = \frac{N^S_{SIS}n_{SIS}}{V^S_{SIS}} = \frac{N^I_{SIS}n_{SIS}}{V^I_{SIS}} = \frac{N^S_{SI}n_{SI}}{V^S_{SI}} = \frac{N^I_{SI}n_{SI}}{V^I_{SI}} = \rho_{S0} = \rho_{I0} = \rho_0 \quad (6a)$$

(b) For the SIS/resin systems:

$$\frac{N_{SIS}n_{SIS}}{V_{SIS}} = \frac{N^S_{SIS}n_{SIS}}{V^S_{SIS}} = \frac{N^I_{SIS}n_{SIS}}{V^I_{SIS}} = \frac{n_R}{V^R} = \rho_{S0} = \rho_{I0} = \rho_{R0} = \rho_0 \quad (6b)$$

We would like once more to point out that the only parameter defining a common length scale between the real and the mesoscopic systems is the gyration radius of the chains. The length of the mesoscopic segment by itself has no physical meaning in our mapping procedure. In this context, when working with SIS/SI blends or SIS/SI/resin solutions, it is possible that the lengths of the mesoscopic chain segments representing the same substance (PS or PI in our case) may depend on whether the PS (or the PI) belongs to a triblock or a diblock molecule.

After the definition of the invariant quantities and the suitable parametrization, it is possible to describe the SBC systems in terms of statistical mechanics using a path integral formalism which can be further treated under the SCF approximation, as has been thoroughly discussed in numerous works and reviews.[11,12,14,29,31,32] The essence of the SCF approach[29] is that the system of interacting polymer chains is replaced by a system of noninteracting polymer molecules considered as random walks in some position-dependent chemical potential fields. These fields affect the conformations of polymer chains defining the spatial distribution of the components of the polymeric system. However, in turn, the chemical potential fields depend on the distribution of the various components in some self-consistent way, so the whole approach boils down to determining the fields that are consistent with the spatial distribution of polymer that they create.

For the case of SIS/SI/resin mixtures it is possible to prove that, within the SCF approach, the free (Helmholtz) energy of the SIS/SI/resin system referred to the total number of molecules will be

$$\frac{\beta F}{\sum_{A=\{SIS,SI,R\}} n_A} = -\sum_{A=\{SIS,SI,R\}} \left\{ \frac{n_A \ln(Q_A/V)}{\sum_{B=\{SIS,SI,R\}} n_B} \right\} + \sum_{A=\{S,I,R\}} \sum_{B=\{S,I,R\}} \frac{\chi_{AB}\langle N\rangle}{2} \int d\mathbf{r}\, \varphi_A(\mathbf{r})\, \varphi_B(\mathbf{r}) - \sum_{A=\{S,I,R\}} \int d\mathbf{r}\, w_A(\mathbf{r})\, \varphi_A(\mathbf{r}) - \int d\mathbf{r}\, \xi(\mathbf{r})\left[1 - \sum_{A=\{S,I,R\}} \varphi_A(\mathbf{r})\right] \quad (7)$$

The φ_A's denote the volume fractions of the three species (styrene, polyisoprene, and resin) and are coupled to the fields $w_A(\mathbf{r})$ through a set of equations:

$$\begin{aligned} \chi_{SI}\langle N\rangle\varphi_I(\mathbf{r}) + \chi_{SR}\langle N\rangle\varphi_R(\mathbf{r}) + \xi(\mathbf{r}) - w_S(\mathbf{r}) &= 0 \\ \chi_{SI}\langle N\rangle\varphi_S(\mathbf{r}) + \chi_{IR}\langle N\rangle\varphi_R(\mathbf{r}) + \xi(\mathbf{r}) - w_I(\mathbf{r}) &= 0 \\ \chi_{SR}\langle N\rangle\varphi_S(\mathbf{r}) + \chi_{IR}\langle N\rangle\varphi_I(\mathbf{r}) + \xi(\mathbf{r}) - w_R(\mathbf{r}) &= 0 \\ \varphi_S(\mathbf{r}) + \varphi_I(\mathbf{r}) + \varphi_R(\mathbf{r}) &= 1 \end{aligned} \qquad (8)$$

$$\varphi_S(\mathbf{r}) = \frac{\tilde{n}_{SIS}N_{SIS}V}{\langle N\rangle} \times \frac{\int_0^{f_{SIS}} ds\, q(\mathbf{r},s)\, q^+(\mathbf{r},s) + \int_{1-f_{SIS}}^1 ds\, q(\mathbf{r},s)\, q^+(\mathbf{r},s)}{Q_{SIS}} + \frac{\tilde{n}_{SI}N_{SI}V}{\langle N\rangle} \frac{\int_0^{f_{SI}} ds\, q(\mathbf{r},s)\, q^+(\mathbf{r},s)}{Q_{SI}}$$

$$\varphi_I(\mathbf{r}) = \frac{\tilde{n}_{SIS}N_{SIS}V}{\langle N\rangle}\frac{\int_{f_{SIS}}^{1-f_{SIS}} ds\, q(\mathbf{r},s)\, q^+(\mathbf{r},s)}{Q_{SIS}} + \frac{\tilde{n}_{SI}N_{SI}V}{\langle N\rangle}\frac{\int_{f_{SI}}^{1} ds\, q(\mathbf{r},s)\, q^+(\mathbf{r},s)}{Q_{SI}}$$

$$\varphi_R(\mathbf{r}) = \frac{\tilde{n}_R V}{\langle N\rangle}\frac{\exp\left(\frac{-w_R(\mathbf{r})}{\langle N\rangle}\right)}{Q_R}$$

The additional field $\xi(\mathbf{r})$ appearing in the free energy functional as well as in eqs 8 is associated with the total incompressibility constraint imposed on SBC materials, while the quantities $\tilde{n}_{SIS}$, $\tilde{n}_{SI}$, and $\tilde{n}_R$ denote the mole fractions of SIS, SI, and R molecules; for example, $\tilde{n}_{SIS} = n_{SIS}/(n_{SIS} + n_{SI} + n_R)$. The parameter $\langle N\rangle$ has the meaning of a mean molecule length and is defined through

$$\langle N\rangle = N_{SIS}\tilde{n}_{SIS} + N_{SI}\tilde{n}_{SI} + \tilde{n}_R \tag{9}$$

The effect of the fields on polymer chain conformations is incorporated in the quantities $q_{SIS}(\mathbf{r},s)$, $q_{SI}(\mathbf{r},s)$, $q^+_{SIS}(\mathbf{r},s)$, and $q^+_{SI}(\mathbf{r},s)$. In particular, $q_{SIS}(\mathbf{r},s)$ and $q_{SI}(\mathbf{r},s)$ are single-chain partition functions of the $(0,s)$ portion of SIS and SI chains, respectively, with the restriction that the segment at fractional contour length s is at the position[33] $\mathbf{r}$. They satisfy the diffusion equations:

$$\frac{\partial q_{SIS}(\mathbf{r},s)}{\partial s} = \begin{cases} \frac{1}{f_{SIS}}R^2_{gS}(SIS)\nabla^2 q_{SIS}(\mathbf{r},s) - \frac{N_{SIS}}{\langle N\rangle}w_S(\mathbf{r})\, q_{SIS}(\mathbf{r},s), & s < f_{SIS} \\ \frac{1}{1-2f_{SIS}}R^2_{gI}(SIS)\nabla^2 q_{SIS}(\mathbf{r},s) - \frac{N_{SIS}}{\langle N\rangle}w_I(\mathbf{r})\, q_{SIS}(\mathbf{r},s), & f_{SIS} < s < 1-f_{SIS} \\ \frac{1}{f_{SIS}}R^2_{gS}(SIS)\nabla^2 q_{SIS}(\mathbf{r},s) - \frac{N_{SIS}}{\langle N\rangle}w_S(\mathbf{r})\, q_{SIS}(\mathbf{r},s), & 1-f_{SIS} < s < 1 \end{cases} \tag{10a}$$

$$\frac{\partial q_{SI}(\mathbf{r},s)}{\partial s} = \begin{cases} \frac{1}{f_{SI}}R^2_{gS}(SI)\nabla^2 q_{SI}(\mathbf{r},s) - \frac{N_{SI}}{\langle N\rangle}w_S(\mathbf{r})\, q_{SI}(\mathbf{r},s), & s < f_{SI} \\ \frac{1}{1-f_{SI}}R^2_{gI}(SI)\nabla^2 q_{SI}(\mathbf{r},s) - \frac{N_{SI}}{\langle N\rangle}w_I(\mathbf{r})\, q_{SI}(\mathbf{r},s), & f_{SI} < s < 1 \end{cases} \tag{10b}$$

with initial conditions $q_{SIS}(\mathbf{r},0) = 1$ and $q_{SI}(\mathbf{r},0) = 1$.

Similarly, $q^+_{SIS}(\mathbf{r},s)$ and $q^+_{SI}(\mathbf{r},s)$ are the partition functions of the $(s,1)$ portion of the SIS and SI chains, respectively, with the restriction that the segment at fractional contour length s is at the position $\mathbf{r}$. They satisfy diffusion equations almost identical to eq 10 with the difference that the right-hand side is multiplied by a factor of -1, and the initial conditions are[11] $q^+_{SIS}(\mathbf{r},1) = 1$ and $q^+_{SI}(\mathbf{r},1) = 1$. Finally, the symbols Q_A stand for the partition functions of a single SIS, SI, or R molecule in the fields $w_S(\mathbf{r})$, $w_I(\mathbf{r})$, and $w_R(\mathbf{r})$ and can be evaluated[32] through

$$Q_{SIS} = \int d\mathbf{r}\, q_{SIS}(\mathbf{r},1),\ Q_{SI} = \int d\mathbf{r}\, q_{SI}(\mathbf{r},1),\ Q_R = \int d\mathbf{r}\, \exp\left(-\frac{w_R(\mathbf{r})}{\langle N\rangle}\right) \tag{11}$$

Equations 8−11 constitute a closed-form system of SCF equations, the solution of which gives the spatial distribution of the styrene, isoprene, and resin components, expressed by the volume fractions $\varphi_A(\mathbf{r})$, and the conformational properties of the SIS and SI molecules, described by the propagators q and q^+. The SIS/SI blends and SIS/resin solutions can be considered as limiting cases of this general formalism by disregarding in eqs 8−11 the terms that are related either to the diblock (SIS/resin systems) or to the resin component (SIS/SI blends).

It can be immediately appreciated that it is impossible to proceed to the solution of eqs 8−11, without specifying the quantities f_{SIS}, f_{SI}, $\chi_{SI}\langle N\rangle$, $\chi_{SR}\langle N\rangle$, $\chi_{IR}\langle N\rangle$, $N_{SIS}/\langle N\rangle$, $N_{SI}/\langle N\rangle$, and $1/\langle N\rangle$. For a detailed presentation of the transformation of these parameters to functions of only invariant quantities, the interested reader is referred to the Appendix. Here we will just mention that these transformations utilize the invariance of volumes and volume fractions introduced in the beginning of this section. Mathematical transformations lead to final expressions, also presented in the Appendix, allowing for the calculation of these parameters exclusively from some experimentally established properties of SBC materials. This final procedure completes the SCF representation of these systems, and the only remaining practical problem is the solution of the system of eqs 8−11.

4. Solution Method

A well-known and powerful approach for the numerical solution of SCF equations is the spectral method of Matsen and Schick,[11] which, despite its effectiveness, has the disadvantage of requiring a prior specification of the symmetry of the mesophase.[14] Since in some cases of SBC's considered in the present work it was not clear what type of morphology to expect, an alternative and more general numerical approach was chosen: a 3D real-space method originally proposed by Drolet and Fredrickson.[12] This technique was extensively presented in several publications,[12,14,15,17] so we will just mention that it comprises an iterative relaxation scheme requiring at each step the numerical solution of the diffusion equations given, in our case, by eqs 10a and 10b. A model system cell with periodic boundary conditions is set up and then discretized through a regular grid. By setting an additional discretization of the scaled chain contour length [0,1], it is possible to solve the diffusion equations by implementing an alternating direction implicit (ADI) algorithm. For the practical realization of the real-space method, apart from defining the rescaled contour length coordinate s, it is convenient to

rescale the space coordinates x,y,z as well. By introducing a suitable multiplication factor before the Laplace differential operator in eqs 10a and 10b, it is possible to define all lengths in units of $\sqrt{R^2_{gI}(SIS)}$, for example.

The iterative scheme, starting from a random generation of the fields $w_A(\mathbf{r})$, can be viewed as a quench leading the system to an equilibrium state corresponding to a minimum of the free energy. Actually, it is not guaranteed whether the scheme will converge to a global or a local minimum of free energy, so there always exists the possibility that the system will become trapped in some metastable equilibrium state. However, this can be considered as an advantage of the method,[14] since real block copolymer systems are well-known for forming metastable structures depending, for example, on the history of their preparation. An additional problem that may arise with this method, especially in the case of small model system boxes, is that the periodic boundary conditions may bias the mesophase structure by enforcing its accommodation in the periodic cell. To deal with this problem in the case of the periodic structures examined here, calculations were performed for a variety of box edge lengths around a given value, and the box size resulting in the lowest free energy per unit mass upon convergence was chosen as the most appropriate one.

The calculations in the present work were performed in model system boxes with sides ranging from 3.5 to 9 $\sqrt{R^2_{gI}(SIS)}$ units. From the small amount of PS present in the SBC molecules, and taking into account the experimental observations, it was estimated that the expected morphologies in these systems should be three-dimensional patterns characterized by a spatial variation of density in all three space dimensions. This made it necessary to solve the SCF equations in the most general three-dimensional formulation. The real-space discretization was performed by defining a cubic lattice grid with 33−35 nodal points in each direction, while the number of nodes used for the discretization of the diblock and the triblock chain contour lengths was on the order of 150 and 300, respectively. Owing to the implementation of the full three-dimensional space formulation, the field theoretic calculations proved very CPU time demanding in some cases. A typical run on a 2.2 GHz, Intel Pentium 4 processor could take from 2 weeks up to 2 months (depending on the SBC system) to reach an equilibrium state. The equilibration was validated by monitoring several quantities: (a) the relative free energy change between successive iterations, which was considered indicative of an equilibrium state if it was of the order of 10^{-6}; (b) the achievement of the incompressibility condition, which is considered to be satisfied if

$$N_{grid}^{-1}\sum_{i=1}^{N_{grid}}(\varphi_S(\mathbf{r}_i)+\varphi_I(\mathbf{r}_i)+\varphi_R(\mathbf{r}_i)-1)^2 < 10^{-4}$$

where the summation is run over all the grid nodes, N_{grid} being their total number; and (c) the quality of formation and ordering of the PS-rich domains in the microphase separated SBC materials. Ideally, a detailed investigation of each system would require analyzing statistically the results of many independent quenches performed from different randomly generated initial field distributions and for different sizes of the model system box. In our case, CPU time limitations did not allow such an extensive study. On the average we were able to perform five successful quenches for each different SBC system.

Table 2. Experimental Data Supplementary to Those of Table 1, Needed for the Complete Evaluation of SCF Model Parameters

quantity	PS	PI	resin
$\tilde{\rho}_0^{true}$ (g/cm^3)	1.0141	0.85669	1.02
C_∞	10.03	5.6	
$(l^2_{ave})^{1/2}$ (Å)	1.53	1.47	
δ (J/cm^3)$^{1/2}$	18.415	16.676	14.588

Table 3. Values of $\chi_{SI}\rho_0$, $\chi_{SR}\rho_0$, and $\chi_{IR}\rho_0$ Parameters Used, during the SCF Calculations, for Various SBC Materials

systems	$\chi_{SI}\rho_0$ (mol/m^3)	$\chi_{SR}\rho_0$ (mol/m^3)	$\chi_{IR}\rho_0$ (mol/m^3)
SIS/SI blends	1008.4		
SIS/resin	925.8	4481.9	1333.7

5. Systems Modeled and Evaluation of Mapping Parameters

The main properties of all SBC materials that were studied are given in Table 1. All calculations were performed at a temperature of $T = 393$ K (120 °C); according to the experimental procedures followed, this is the relevant temperature for structure formation. The densities of pure polystyrene and pure isoprene needed for the computation of macroscopic volumes (eq A.5) were evaluated from empirical formulas correlating experimental data presented by Mark[34] and Han and Kim,[35] respectively, while the data for the resin density were provided by ExxonMobil. The C_∞ parameters and the mean-squared bond lengths $l^2_{(S)ave}$ and $l^2_{(I)ave}$, needed for the evaluation of the squared gyration radii, eq 2, were calculated from data presented by Mark.[34] Finally, for the evaluation of the $\chi_{AB}\rho_0$ products, both approaches described above were used. In particular, in the TD blends the only parameter of this kind needed is the product $\chi_{SI}\rho_0$, which was computed from the Rounds−McIntire formula, eq 5. In T2R systems the three different nonbonded interactions present require the evaluation of three parameters: $\chi_{SI}\rho_0$, $\chi_{SR}\rho_0$, and $\chi_{IR}\rho_0$. In this case the Hildebrand solubility parameter relationship, eq 4, was used, where the styrene solubility parameters were taken from Helfand-Sapse,[8] while the isoprene and resin solubility parameters were provided by ExxonMobil. The values of all the experimental data mentioned above are summarized in Table 2. For the reader to have a clearer picture concerning the degree of mutual miscibility of the various system components, the values of the parameters $\chi_{SI}\rho_0$, $\chi_{SR}\rho_0$, and $\chi_{IR}\rho_0$ are presented in Table 3. Table 4 contains the values of the parameters $\tilde{n}_{SIS}$, $\tilde{n}_{SI}$, $\tilde{n}_R$, $R^2_{gS}(SIS)$, $R^2_{gI}(SIS)$, $R^2_{gS}(SI)$, $R^2_{gI}(SI)$, $2f_{SIS}$, and f_{SI} used for the mesoscopic representation of the SBC systems.

6. Results

6.1. Microphase Separation and Observed Morphologies. The SCF calculations confirm the experimental observations of formation of PS-rich spherical domains in all pure triblock (T2) and pure diblock (D) melts as well as in all T2D and T3D blends. Figure 1 shows two pictures representative of phase separated melts and blends, obtained by replicating the initial model system cell three times in each direction. For clarity, only the PS-rich regions (regions where the PS

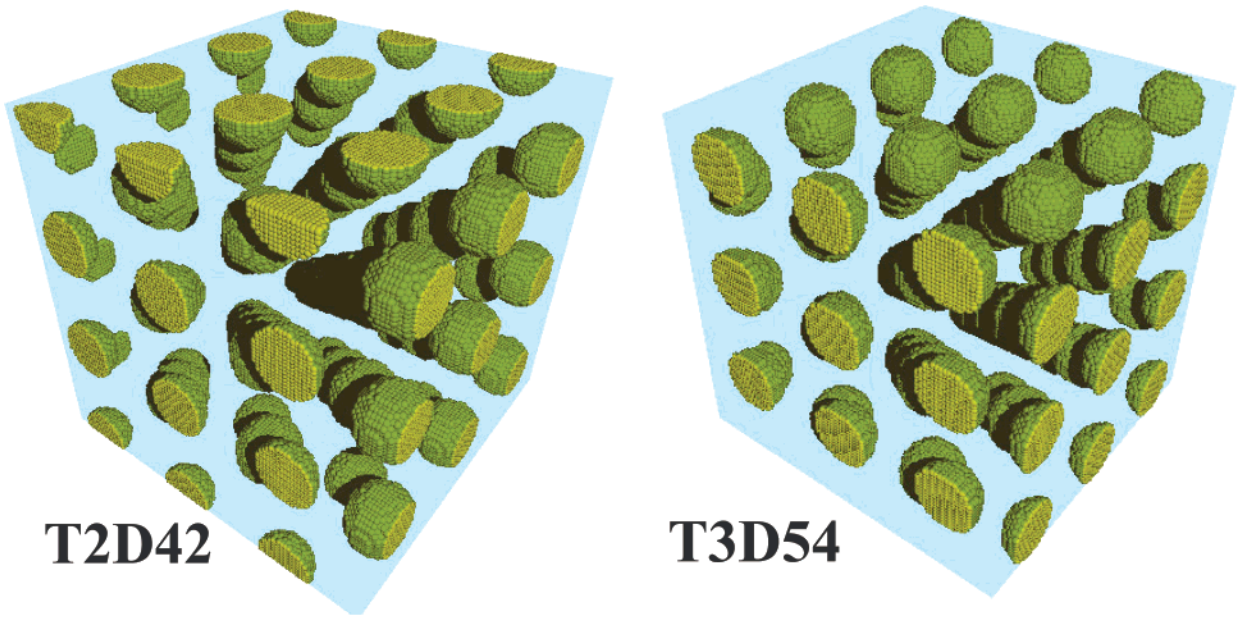

Figure 1. SCF calculation results for a T2D42 (left) and a T3D54 (right) blend forming PS-rich domains [$\varphi_S(\mathbf{r}) > \varphi_I(\mathbf{r})$], which are shown in green. The light blue background represents the PI-rich matrix.

Table 4. Values of the Various Mapping Parameters Used during the Mesoscopic Representation of the SBC Materials

	sample code						
parameter	T2	T2D19	T2D42	T3D54	T2R20	T2R40	T2R60
$\tilde{n}_{SIS}$	1	0.666	0.393	0.743	9.6×10^{-3}	3.6×10^{-3}	1.6×10^{-3}
$\tilde{n}_{SI}$		0.334	0.607	0.257			
$\tilde{n}_R$					0.9904	0.9964	0.9984
R^2_{gS}(SIS) (nm^2)	8.74	8.74	8.74	10.66	8.74	8.74	8.74
R^2_{gI}(SIS) (nm^2)	155.11	155.11	155.11	175.18	155.11	155.11	155.11
R^2_{gS}(SI) (nm^2)		8.12	8.12	8.66			
R^2_{gI}(SI) (nm^2)		72.60	72.60	71.75			
$2f_{SIS}$	0.13	0.13	0.13	0.138	0.13	0.13	0.13
f_{SI}		0.13	0.13	0.138			

volume fraction exceeds 0.5) are shown in green, while the blue background corresponds to the PI-rich matrix.

To clarify whether the PS-rich domains in SBC melts and blends form a long-range ordered structure in space, a Voronoi tessellation[15,33] was performed with respect to the centers of the domains. The shape of the Voronoi cells characterizing the morphologies of microphase separated SBC melts and blends for the majority of quenches performed was identified as a truncated octahedron, indicative of a body-centered-cubic (bcc) arrangement of the spherical domains. Nevertheless, in some cases of SBC's, T2 melts for example, a few quenches led to converged morphologies characterized by a different type of Voronoi polyhedron, identified as a rhombic dodecahedron, characteristic of a face-centered-cubic (fcc) arrangement of the spherical domains. In all cases where an fcc arrangement was observed, the corresponding free energy was higher in comparison to the one of the bcc structure. Therefore, we can argue that the more favorable morphology of the phase separated SBC's studied in this work, in a state of thermodynamic equilibrium, is the bcc one.

Although the Voronoi tessellation is quite illustrative in specifying the type of the long-range order exhibited by the microphase separated T2D and T3D blends, their SAXS spectrum was also evaluated for a direct comparison with the experiments. Since SBC materials are considered as incompressible, the scattered intensity $I(\mathbf{q})$ in SIS/SI blends will be proportional[36] only to the styrene−styrene structure factor $S_{SS}(\mathbf{q})$, defined as

$$S_{SS}(\mathbf{q}) = \int\int \varphi_S(\mathbf{r}_1)\, \varphi_S(\mathbf{r}_1 + \mathbf{R}) \exp(i\mathbf{qR})\, d\mathbf{r}_1\, d\mathbf{R} \quad (12)$$

where $\mathbf{q}$ is the scattering vector. The SAXS spectrum $I(q)$ can be estimated[37] by circularly averaging the structure factor $S_{SS}(\mathbf{q})$:

$$I(q) \sim \frac{1}{4\pi}\int_{|\mathbf{q}|=q} S_{SS}(\mathbf{q})\, d\Omega = \int\int \varphi_S(\mathbf{r}_1)\, \varphi_S(\mathbf{r}_1 + \mathbf{R}) \frac{\sin |\mathbf{q}||\mathbf{R}|}{|\mathbf{q}||\mathbf{R}|} d\mathbf{r}_1\, d\mathbf{R} \quad (13)$$

In this work, the double integral over the vectors $\mathbf{r}_1$ and $\mathbf{R}$ is replaced by a double sum running over all the nodal points of the mesh used during the SCF calculations, where the values of the function $\varphi_S(\mathbf{r})$ are known. To avoid significant small system size effects, the initial model system cell had to be replicated four or five times in each direction before performing the SAXS calculations. The corresponding model SAXS spectra of the T2D blends are shown at the top of Figure 2. For a better understanding of these spectra, the scattering curve of a single PS-rich spherical domain, similar to those that were observed in T2 melts, is also reproduced.

Comparing the theoretically estimated scattering curves of Figure 2 with the experimental SAXS spectra

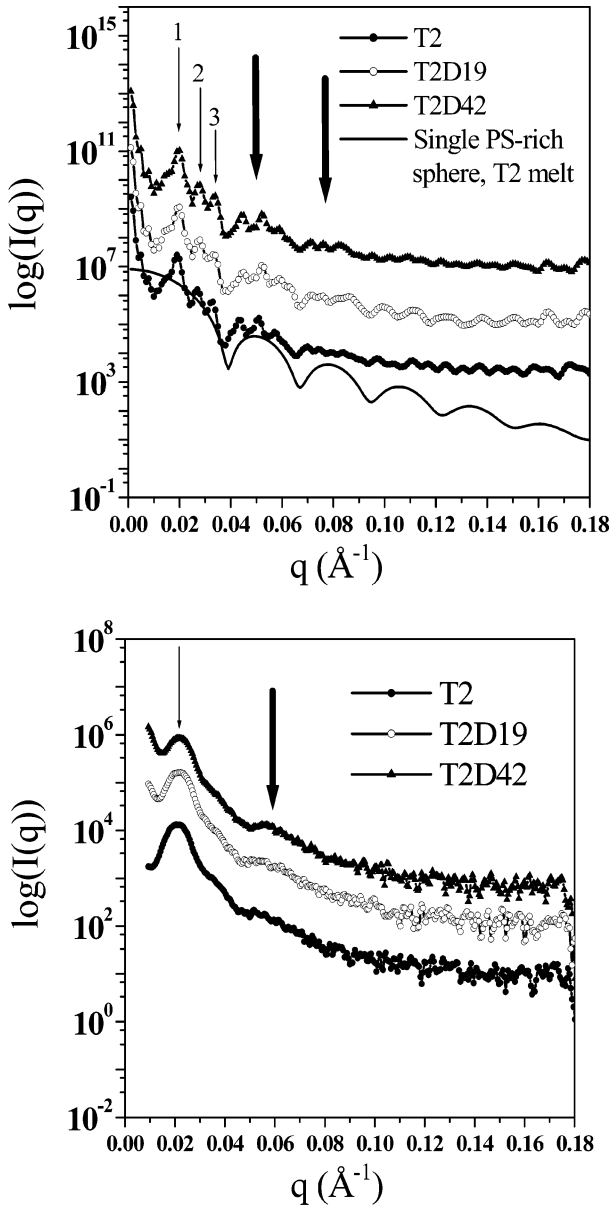

Figure 2. SAXS diagrams for T2, T2D19, and T2D42 blends estimated from SCF results (top) compared to the experimentally obtained SAXS spectra of the same systems (bottom). For clarity, the original SAXS curves are shifted along the vertical axis.

presented at the bottom of the same figure, it can be seen that the SCF calculations agree well with the experimental observation that the scattering peaks should be divided in two groups: those originating from interdomain interference (marked with thin arrows) and those that are due to single PS-rich spherical domain scattering (marked with thick arrows). However, the model SAXS spectra, apart from the first interdomain interference peak (marked as "1"), exhibit several additional secondary maxima due to the regular spatial arrangement of the PS-rich domains in space, confirmed through the Voronoi tessellation. Particularly the bcc arrangement of the PS micelles is evident from the ratios of the q_2 and q_3 values, where the secondary interdomain interference peaks appear, to the value q_1 of the main peak: $q_2/q_1 \approx \sqrt{2}$ and $q_3/q_1 \approx \sqrt{3}$. Contrary to the SCF predictions for all the blends that were studied, the experimental data do not show any other pronounced maxima, apart from the first interdomain interference peak. Instead, there is a wide "shoulder" between the main peak and the maximum due to the single PS-rich sphere scattering, suggesting a liquidlike (disordered) arrangement[38] of the PS micelles in the experimentally realized SBC's. We believe that the reason for this absence of long-range ordered structures should be sought in the preparation history of the test specimens. Indeed, usually in the literature[30] long-range ordered structures are observed in block copolymer melts by first slowly evaporating the solvent from the system and then annealing the test specimen in a vacuum for a very long time at a given temperature.[38] These procedures, necessary to obtain a thermodynamically favorable equilibrium state of the system, can take up to a month. In this work the microphase separated SBC materials were prepared either by following the industrial hot melt procedures or by casting them from toluene solution, without allowing too much time for the system equilibration. Therefore, one should not expect to see so well-developed structures as in the block copolymer systems prepared by slow solvent evaporation and prolonged annealing. This explanation is actually supported by the observation that the SBC's prepared from toluene seem to be better structured than those materials that were prepared with the hot-melt technique.

The field theoretical modeling of imperfectly formed structures observed in the experiments presents an interesting (and still open, to the best of our knowledge) problem, since it is not yet clear how to compel the numerical procedure to converge to the particular state of the experimental samples. In an attempt to mimic the imperfect structure formation seen in experiment, the SCF calculations were performed on large calculation cells, allowing an easy entrapment of the system in a local minimum of the free energy. As an example, a morphology obtained in a cell with an edge length of $7\sqrt{R_{gI}^2(\mathrm{SIS})}$ units and 33 nodal points discretization in each direction is shown on the left of Figure 3. In this case, the PS-rich domains look like irregularly shaped clusters exhibiting no long-range order in space. Actually, this picture agrees well with the AFM image of a T2 melt shown on the right of Figure 3. The corresponding model SAXS spectrum is shown in Figure 4. The well-developed secondary interdomain interference scattering peaks have disappeared in this case due to the liquidlike ordering in space of the PS-rich clusters, while the maximum due to single PS-rich domain scattering has become considerably less pronounced and very broad. The reasons should be sought in the imperfect shape of the PS-rich domains as well as in the "polydispersity" of their size: the gyration radii of the PS-rich clusters in the structure shown in Figure 3 were found to vary from 11.5 to 21.5 nm.

To support that the state in which the system becomes "locked" after solving the SCF formalism in large model system boxes is not just an artifact of the numerical method, but indeed corresponds to a well-defined metastable state, the calculations were repeated for several box lengths varying from 7 to 9 $\sqrt{R_{gI}^2(\mathrm{SIS})}$ units. Although the free energies of the different structures obtained in this way could differ up to 0.5%, which may be important,[11] it was observed that in all cases the properties of the morphologies were very similar. To visualize this, we present, in Figure 5, three typical model AFM "slices", obtained for three simulation box

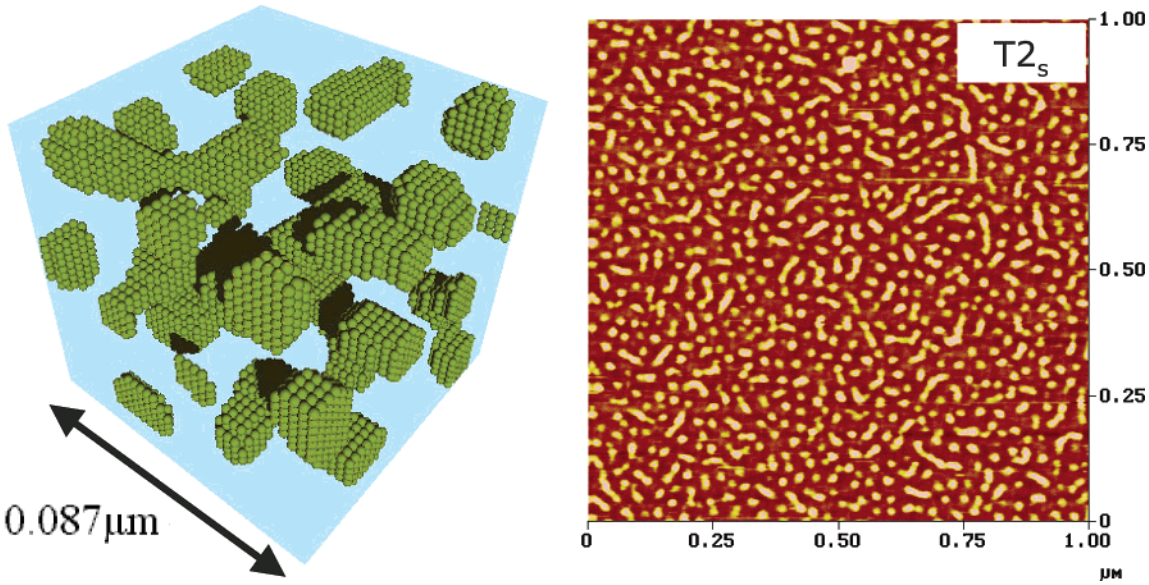

Figure 3. SCF calculation results (left) for a T2 melt performed in a large model system box (7 $\sqrt{R^2_{gI}(SIS)}$ units), showing an imperfectly formed PS-rich domain [$\varphi_S(\mathbf{r}) > \varphi_I(\mathbf{r})$] structure. On the right is shown an AFM image of the same system.

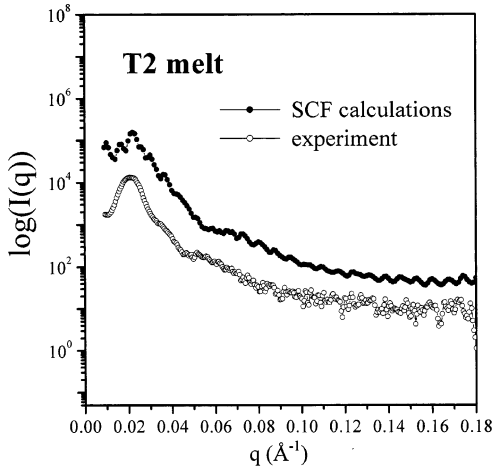

Figure 4. Model SAXS pattern (solid circles) for the microphase separated T2 blend shown in Figure 3. On the same graph the experimental SAXS spectrum (open circles) is also reproduced.

sizes: 7, 8, and 9 $\sqrt{R^2_{gI}(SIS)}$ units. Clearly, the slices resemble each other closely. The similarity of the structures is further quantified in Figure 6, which shows the model SAXS spectra (top) and the spatial correlation functions (bottom) of styrene volume fraction: $G_{SS}(R) = \langle \phi_S(\mathbf{0})\ \phi_S(\mathbf{R}) \rangle$ for all the three large systems reported above. It can be observed that indeed these quantities for all the numerically obtained metastable states follow the same behavior. This provides strong indication that the disordered configurations obtained through our SCF calculations are representative of very similar metastable thermodynamic states with the same statistical properties. Their close resemblance to the experimentally obtained configurations supports the idea that the latter are not unstable, frozen-in at some arbitrary point on their way to equilibrium, but actual metastable states.

The effect of resin content on microphase separation in SIS/resin solutions is more complicated. SCF calculations agree well with experimental evidence for the formation of spherical morphologies in systems with low resin content, such as T2R20. SCF predicts that microphase separation should take place, leading to well-formed PS-rich spherical domains arranged on a bcc lattice. An example of such a phase-separated T2R20 morphology, obtained by replicating the calculation cell three times in each direction, is shown on the left of Figure 7. The corresponding Voronoi unit cell, a truncated octahedron, is shown boxed in the middle of the same figure.

As the resin content is increased, SCF theory predicts that microphase separation should still take place, leading to the formation of PS-rich spherical-like domains. These were observed during the calculations performed for T2R60 solutions, although the corresponding experimental evidence obtained by different methods is contradictory. In particular, although the SAXS spectrum of T2R60 reveals the presence of some structure, it was impossible to confirm this by AFM.

These experimental difficulties may be consistent with the observation that, in the framework of the numerical method implemented in our calculations, although the phase separation took place easily in T2R60, no well-organized long-range order morphology was ever formed. Actually, from the data accumulated during this study, it is impossible to conclude whether a minimum of free energy corresponding to an equilibrium state can be reached, where the spherical domains in T2R60 systems form a long-range ordered structure. It could be argued that this difficulty in observing well-organized structures in T2R60 solutions might be an indication of the inefficiency of the 3D real-space method, as implemented in this work, to handle these systems properly. On the other hand, apart from the SAXS and AFM measurements indicating the absence of long-range order in these phase separated systems, these SCF predictions are also consistent with other experimental data reported in the literature.[39] We present on the right of Figure 7 a microphase separated structure of a T2R60 system, which could correspond to an experimentally realizable state since all the physical requirements (the incompressibility condition, the percentage of the various components) are fulfilled. The absence of a well-structured morphology is evident,

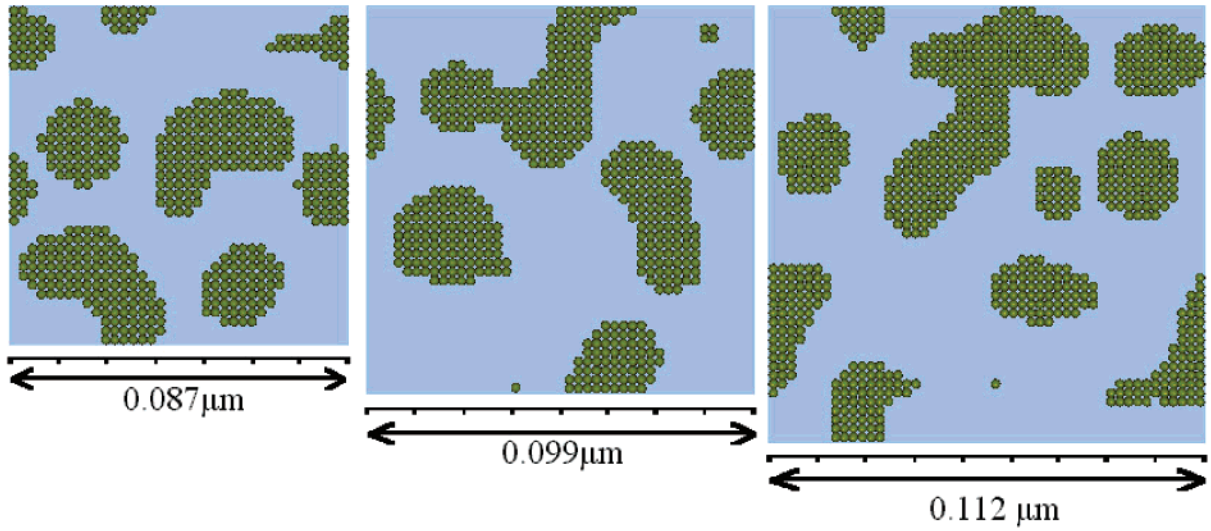

Figure 5. Typical model AFM images of a T2 melt calculated for three different large model system boxes with edge lengths of 0.087, 0.099, and 0.122 μm, corresponding to 7, 8, and 9 $\sqrt{R^2_{gI}(SIS)}$ units, respectively.

Table 5. Comparison of Values of the Smallest Distance between the Centers of Neighboring Polystyrene Domains, d_1, and the Diameter of Polystyrene Domains, d_2, As Obtained from SCF and As Measured with SAXS

systems studied	SCF		experiment	
	d_2 (nm)	d_1 (nm)	d_2 (nm)	d_1 (nm)
D	16.5	31		
T2	20.8	39.5	22	30
T2D19	19.8	38.7	22	30
T2D42	21	38.6	22	30
T3D54	18	34.3		
T2R20	18.4	36.47	22	30−31
T2R60	14	20		30

although the formation of PS-rich spherical-like micelles can clearly be seen.

6.2. Characterization of the Observed Morphologies. After the determination of the types of morphologies observed in microphase separated SBC materials, it is possible to evaluate the size (diameter) of the spherical domains, d_2, as well as the smallest distance between their centers, d_1. These data were also estimated from SAXS measurements, so they provide a good basis for a comparison with SCF predictions. The theoretical and the experimental data are presented in Table 5.

It can be seen that the d_1 and d_2 parameters calculated by SCF theory in T2 melts, in SIS/SI blends, and in the T2R20 solution are in satisfactory qualitative agreement with the experimental data. We believe that the somewhat higher values of the SCF predictions for the d_1 lengths in comparison with the experimental ones originate, mainly, from the fact that the experimental samples do not exhibit any long-range order, being characterized by a "liquidlike" arrangement of the PS-rich domains. In this context they present a different type of morphology, and they should not be expected to have the same characteristics with the bcc structures. This is supported by the fact that all SCF calculations performed for T2 melts on large model system boxes gave randomly ordered PS-rich domains characterized by an interdomain spacing, d_1, of 32 nm while their size, d_2, was close to 19 nm (see the $G_{SS}(R)$ spatial correlation function reported at the bottom of Figure 6). Both values in this case are close to the corresponding experimental data.

Nevertheless, it was possible to reproduce the experimentally observed trends in the behavior of the characteristic lengths as a function of diblock and resin content. In particular, it can be seen that the values of characteristic lengths are practically indifferent to diblock and to small resin (T2R20 solutions) contents. Only the pure diblock (D) melt is characterized by perceptibly smaller d_1 and d_2 parameters. Considering that the block copolymers composing the blends are selected in such a way that the diblock is actually a little less than the triblock molecule split in half, the above behavior is consistent with previous SCF calculations performed using the spectral method of Matsen and Shick.[11] Indeed, in the work of Matsen and Thompson,[33] model ABA triblock melts were studied, and their properties were compared to those of an AB diblock melt where the molecules were corresponding to triblock chains cut in half. In that case it was established that the period of the triblock morphology should be by about 5% larger than the one of the corresponding diblock melt. It is also interesting to see that, by increasing the diblock percentage in the blend, the morphology characteristics are driven toward the ones of the D melt. This is in accord with experimental observations reported by Hadziioannou and Skoulios,[40] where SIS and SI blends were also considered.

As was discussed above, in T2R60 solutions we recorded the absence of a long-range order in the microphase separated morphologies obtained from SCF. In this case, just as in the T2 melts with liquidlike ordering of PS-rich domains, the d_1 parameter characterizes the distance between the nearest-neighbor domains. During the calculation of d_2, a significant scatter of the size of the spherical-like PS-rich domains around the mean value was recorded: although the mean d_2 reported in Table 5 was about 14 nm, the size of the individual domains was seen to vary considerably from 7.5 to 44 nm around this value.

6.3. Polymer and Resin Distribution in Microphase Separated Systems. Apart from identifying the type and determining the characteristic lengths of the observed morphologies in SBC's, the profiles of volume fractions of the various components (styrene, isoprene, and resin) in the PS-rich domains were also

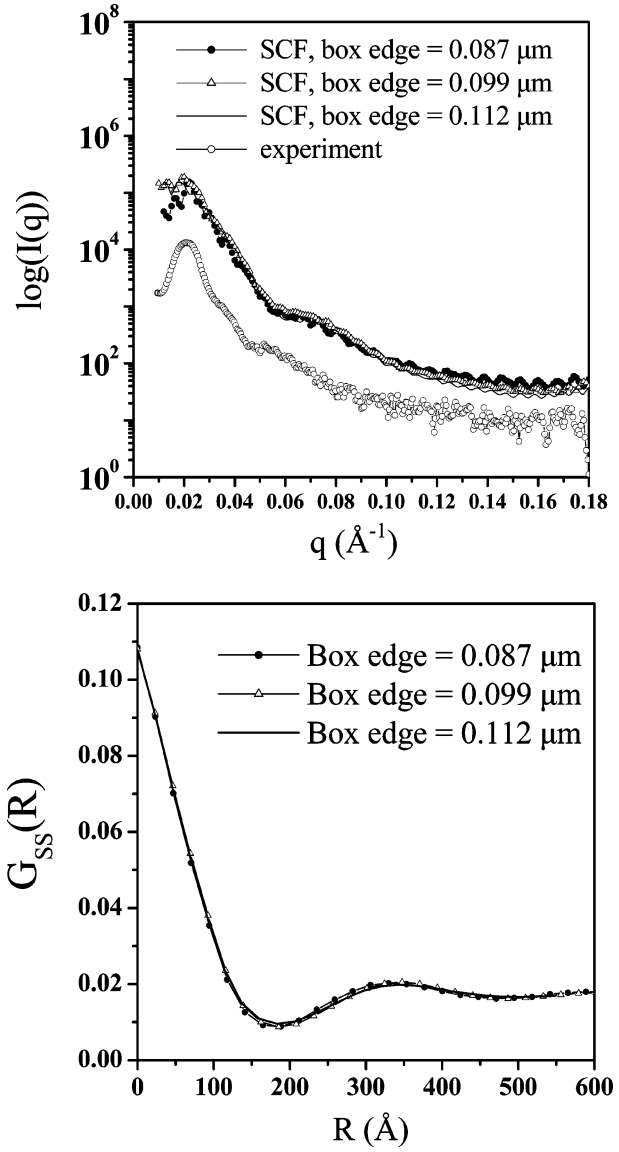

Figure 6. Model SAXS patterns (top) for a T2 melt estimated from SCF calculations performed for three different large model system boxes with edge lengths of 0.087, 0.099, and 0.122 μm, corresponding to 7, 8, and 9 $\sqrt{R_{gI}^2(\mathrm{SIS})}$ units, respectively. The spatial correlation functions of styrene volume fraction, $G_{SS}(R) = \langle \phi_S(\mathbf{0})\, \phi_S(\mathbf{R}) \rangle$, calculated for these three large systems, are reported at the bottom of the same figure.

evaluated along the axis passing from the centers of these domains. The volume fraction profiles obtained for T2, T2D19, T2D42, and T2R20 systems with the corresponding PS-rich sphere sketched underneath for clarity are shown in Figure 8.

The strong segregation of the T2 melt and the TD blends is evident from the negligible amount of isoprene entering the spherical PS-rich domain. The interfacial width in T2 melts is estimated at 3.5 nm, in qualitative agreement with the data reported in the literature.[41] For the case of blends, it is observed that the distribution of the polystyrene belonging to different kinds of molecules (diblock or triblock) is not uniform in the PS-rich micelles: the PS strands of the diblock molecules exhibit a slight preference to occupy the outer core of the PS sphere, while the triblock PS end-blocks prefer to assemble in the center. Interestingly, in the T2R solutions, although the resin is a selective solvent for the PI blocks, some amount of it ranging from 5 to 10% in volume can be detected in the PS-rich spheres as well. Similar behavior has been reported for other triblock/solvent systems where the selective solvent for the middle block could be also detected in the micelles formed by the end blocks.[39]

This presence of resin in the PS micelles is not innocuous from the point of view of the properties, since it can modify the glass transition temperature (T_g) of the styrene micelles. Depending on the T_g of the resin (typically 40−50 °C) or plasticizers ($T_g \sim -20$ °C) which are used, the useful temperature range where the PS domains can act as effective physical cross-links could be reduced. Since this temperature resistance is an important limitation of SBC based adhesives, it would be particularly useful to be able to predict what volume fraction of resin or plasticizer is present in the styrene phase and to deduce then from the composition the glass transition temperature of the styrene spheres. This information is extremely difficult to obtain reliably experimentally when the volume fraction of styrene falls below 10%, as is typically the case in PSA. Our results are therefore very promising in this direction.

6.4. Bridging Properties of SIS Molecules. The numbers of SIS molecules acting as bridges between the PS micelles in the microphase-separated SBC's can be evaluated utilizing the equilibrium values of the mean fields $w_A(\mathbf{r})$ obtained from the SCF calculations. A straightforward procedure for performing this evaluation based on the Voronoi tessellation mentioned above was introduced by Matsen and Thompson.[33] Apart from this well-known method, there is an alternative approach particularly suitable for those cases where it is difficult to define some reference points in the structure for performing the Voronoi tessellation. This can happen, for example, in microphase separated systems where the shape of domains is not well-defined: T2R60 solutions in our case. This approach uses some small threshold value of the polystyrene volume fraction (0.01 for example) to define the PS-rich domains. Then, a SIS molecule is considered in a looped conformation if both junctions between the PI middle-block and two PS end-blocks are found in the same domain, denoted as D, while it forms a bridge in all other cases. The procedure[15,33] follows closely the approach of Matsen and Thompson and is based on the definition of the function

$$\bar{q}(\mathbf{r}, s = f_{SIS}) = \begin{cases} q(\mathbf{r}, s = f_{SIS}) & \mathbf{r} \in D \\ 0 & \mathbf{r} \notin D \end{cases} \qquad (14)$$

where $q(\mathbf{r},s=f_{SIS})$ is obtained by solving the diffusion equation (10a). The function $\bar{q}(\mathbf{r},s=f_{SIS})$ is then propagated with the diffusion equation (10a) to obtain its value at $s = 1 - f_{SIS}$. The nonnormalized probability that the junction $1 - f_{SIS}$ of the SIS chain is found at $\mathbf{r}$, provided that junction f_{SIS} is in the domain D, will equal the product $\bar{q}(\mathbf{r},1 - f_{SIS})q^+(\mathbf{r},1 - f_{SIS})$, so the loop fraction will be

$$f_{loop} = \frac{\int_D \mathrm{d}\mathbf{r}\ \bar{q}(\mathbf{r},1 - f_{SIS})q^+(\mathbf{r},1 - f_{SIS})}{\int_V \mathrm{d}\mathbf{r}\ \bar{q}(\mathbf{r},1 - f_{SIS})q^+(\mathbf{r},1 - f_{SIS})} \qquad (15)$$

The fraction of bridges can be then evaluated as $f_{bridges} = 1 - f_{loop}$.

Both methods are consistent with each other, giving for all the SBC's practically the same results for the

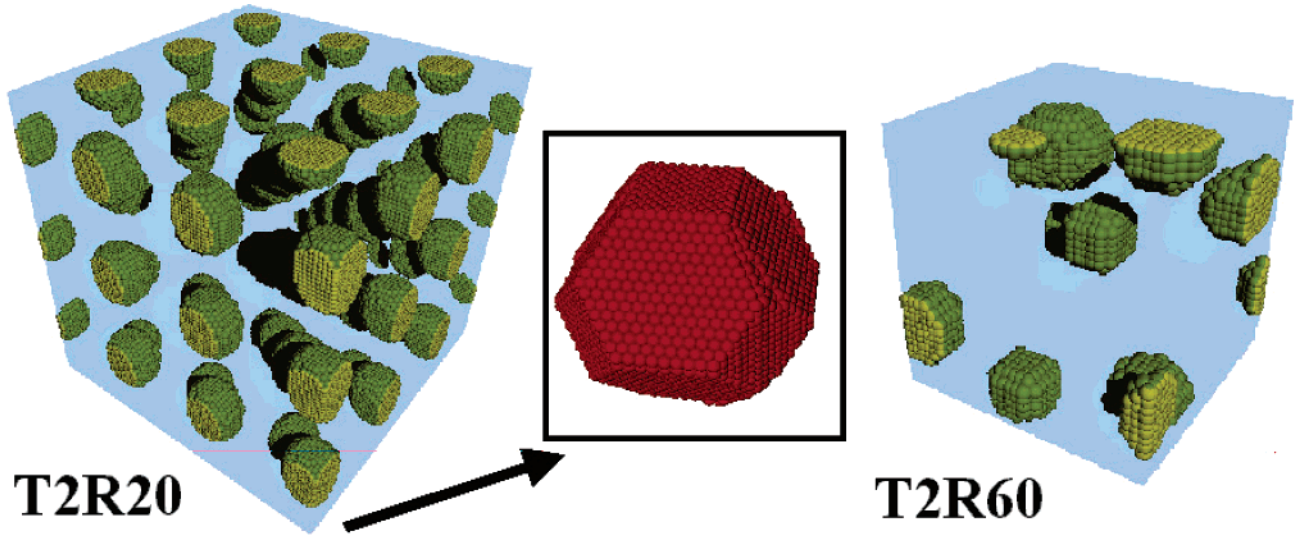

Figure 7. SCF theory results for a T2R20 (left) and a T2R60 (right) system with PS-rich domains [$\varphi_S(\mathbf{r}) > \varphi_I(\mathbf{r})$] shown in green color. The Voronoi cell, shown boxed in the middle, proves the bcc arrangement of the spherical micelles in the T2R20 system.

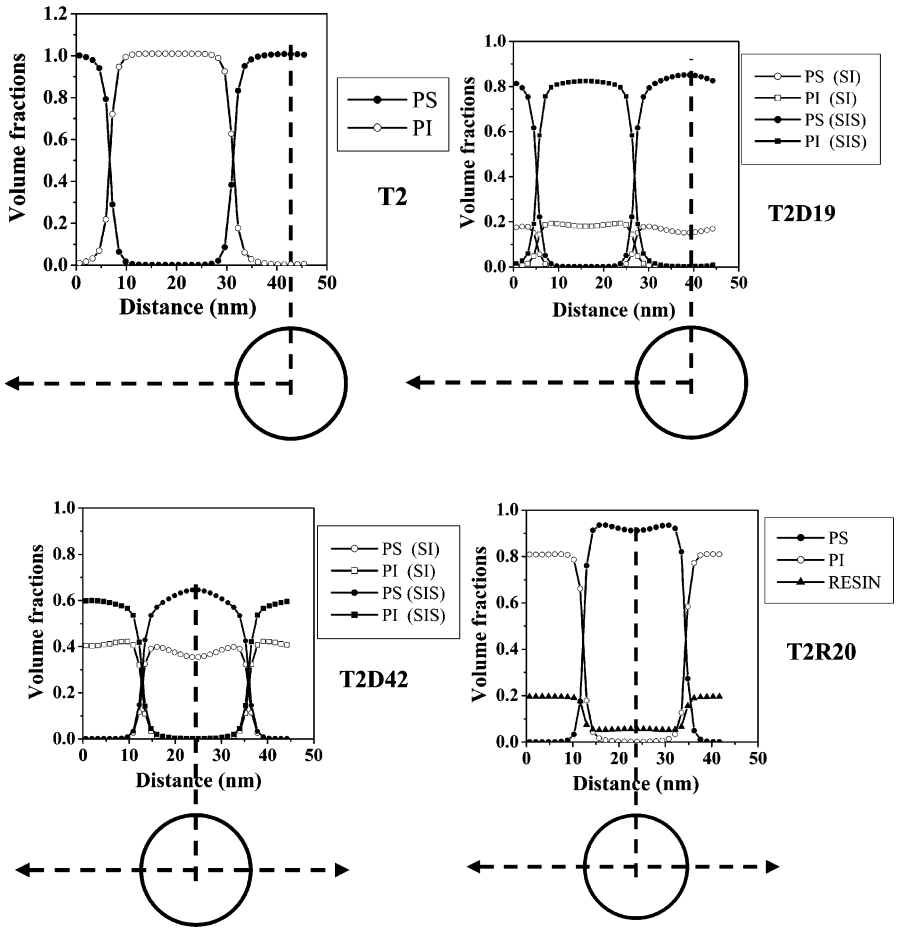

Figure 8. Volume fraction profiles for the styrene, isoprene, and resin components calculated by SCF for the various SBC systems.

percentage of SIS molecules forming bridges. These are presented in Table 6. It is observed that for the SIS triblock melts (T2 systems) the percentage of molecules forming bridges is 79%, which is in accordance with other SCF calculations[33] performed for model ABA systems. The general conclusion from the data shown is that, in all SBC systems that were simulated, the percent of SIS molecules acting as bridges is roughly 80% of their total number and is practically invariant with the diblock or resin percentage. The only exception is the T2R60 solutions, where the percentage of SIS molecules forming bridges is somewhat higher, 90% of their total number.

6.4. Mechanical Properties of SBC Systems. After establishing the bridging properties of SIS molecules in SBC materials, a rubber elasticity theory can be utilized to predict their shear modulus by considering the PS domains as cross-linking points in a network formed by the triblock polymer chains. As a first approximation, one could try the standard affine theory of rubber

Table 6. SCF Results Concerning the (a) Bridging Fraction of SIS Molecules, (b) Number of Bridges per Unit Volume, (c) G_c Shear Modulus (Cross-Link Contribution), and (d) G_e Shear Modulus (Entanglement Contribution) in Various SBC Systems[a]

systems studied	$f_{bridges}$ (%)	n_{bridge} (mol/m^3)	G_c(MPa)		G_e (MPa)	
			forward	regressive	forward	regressive
T2	79	4.78	0.0117	0.1145	0.5699	0.4397
T2D19	78.5	3.84	0.0094	0.0520	0.4615	0.4386
T2D42	79.4	2.78	0.0068	0.0180	0.3303	0.3661
T3D54	84.5	2.05	0.0050	0.0014	0.2602	0.3333
T2R20	80.4	3.99	0.0097		0.3525	
T2R60	90	2.35	0.0057	0.0328	0.0739	0.0757

[a]For each of the G_c and G_e moduli the results of the direct (forward) and the fitting (regressive) calculations are reported.

elasticity, according to which the shear modulus G_c and the nominal stress−strain, $\sigma(\epsilon)$, relationship are given by

$$G_c = n_{bridge}RT, \quad \sigma(\epsilon) = G_c\left(1 + \epsilon - \frac{1}{(1+\epsilon)^2}\right) \quad (16)$$

where n_{bridge} (mol/m^3) is the total number of bridges per unit volume. Since the SBC's studied here are strongly segregated systems, all the PS end-blocks will be distributed among the micelles, and the n_{bridge} will be given by

$$n_{bridge}\ (\text{mol/m}^3) = \frac{\varphi f_{bridges}}{V_{molar}^{SIS}} \quad (17)$$

where φ is the volume fraction of SIS in the system and V_{molar}^{SIS} is the molar volume of SIS. The results of this calculation for all the systems studied are presented in Table 6.

However, after substituting these values for G_c into eq 16, one immediately comes up with stresses that are smaller than the experimentally measured values by at least 1 order of magnitude. This contradiction is partially resolved by realizing that the G_c estimated through these crude theoretical arguments should not be considered as the total shear modulus of the SBC systems. Simple rubber elasticity theory is not taking into account the role of entanglements between the polymer chains forming the network. Therefore, the G_c expresses only the cross-link contribution to the shear modulus; the fact that it differs significantly from the total shear modulus measured in the tensile tests underlines the crucial role of entanglements in determining the SBC mechanical properties. This role is easily understood if one considers that the average molecular weight between entanglements for PI chains is of the order of 4 kg/mol, 30 times less than the molecular weight of a PI bridge between two PS domains.

Since standard affine rubber elasticity theory does not take into account the presence of entanglements, several refinements and modifications have since been developed. A particularly illuminating one, in terms of physical mechanisms, is the slip-tube model of Rubinstein and Panyukov[21] predicting the following expression for the stress−strain, $\sigma(\epsilon)$, relationship:[21]

$$\frac{\sigma(\epsilon)}{1 + \epsilon - \frac{1}{(1+\epsilon)^2}} = G_c + G_e/(0.74(1+\epsilon) + 0.61(1+\epsilon)^{-1/2} - 0.35) \quad (18)$$

where G_c and G_e represent the part of the elastic modulus due to the phantom network (fixed) and the part due to the entanglements, respectively, and are given by[21]

$$G_c = RTn_{bridge}(1 - 2/\varphi_{network}), \quad G_e = RTc/N_e \quad (19)$$

where c, $\varphi_{network}$, and N_e are the monomer concentration, functionality of network cross-links, and number of monomers between entanglements in the polymer melt, respectively. Equation 18 with the definitions of G_c and G_e, eq 19, constitutes a closed expression that is used here to describe the elastic properties of SBC materials in two ways: (a) a direct (we will call it "forward") approach, which consists of estimating the two moduli, G_c and G_e, from SCF results and molecular characteristics of the components of the SBC materials, and (b) a "regressive" approach, treating G_c and G_e as fitting parameters to obtain the best description of the experimental tensile data by the slip-tube model functional form of eq 18.

Key points of the "forward" approach are the determination of the entanglement length, N_e, and the monomer concentration, c. If MW_{SIS} is the molecular weight of the SIS triblock, then in pure T2 melts the number density of PI blocks in the system[21] is $\nu_{PI} = \tilde{\rho}_{I0}^{true}/[MW_{SIS}(1 - \alpha_{SIS})]$. All PI blocks of the triblock molecules contribute to the entanglement structure, since all are tethered to rigid polystyrene domains on both ends. G_e can be evaluated after some trivial mathematical operations:

$$G_e = RT\frac{N_{SIS}}{N_e}(1 - f_{SIS})\nu_{PI} = RT\frac{\tilde{\rho}_{I0}^{true}}{MW_e(PI)} \quad (20)$$

where MW_e(PI) is the PI entanglement molecular weight, while it is assumed that

$$N_{SIS}(1 - f_{SIS})/N_e = MW_{SIS}(1 - \alpha_{SIS})/MW_e(PI) \quad (21)$$

In this way, the only parameters related to the molecular structure of the polymer chains involved in the evaluation of G_e are (a) the density $\tilde{\rho}_{I0}^{true} = 0.914$ g/cm^3 and (b) the entanglement molecular weight $MW_e(PI) = 3937$ g/mol, calculated for temperature $T = 293$ K from empirical formulas presented by Mark.[34]

For the calculation of G_e in T2R systems it should considered that the contour length $N_e^{solution}$ between entanglements in the semidilute solutions constituting the resin-swollen polyisoprene increases with decreasing volume fraction of the polyisoprene, φ_{PI}, according to

the power law[42] $N_e^{solution} \sim N_e \phi_{PI}^{-5/4}$. In accordance with this, the G_e will be given by

$$G_e = RT\frac{N_{SIS}}{N_e}(1 - f_{SIS})\phi_{PI}^{5/4}\nu_{PI} = RT\,\frac{MW_{SIS}(1 - \alpha_{SIS})\phi_{PI}^{5/4}\nu_{PI}}{MW_e(PI)} \quad (22)$$

where the assumption of eq 21 was invoked. Taking into account that $\nu_{PI} = \phi_{PI}\tilde{\rho}_{I0}^{true}/MW_{SIS}(1 - \alpha_{SIS})$, the final expression for G_e becomes

$$G_e = RT\,\frac{\phi_{PI}^{9/4}\tilde{\rho}_{I0}^{true}}{MW_e(PI)} \quad (23)$$

according to which G_e should scale as $\phi_{PI}^{2.25}$ with PI volume fraction. Interestingly, this result is in full accordance with de Gennes' prediction concerning the power law dependence of the elastic modulus on the concentration of polymer in semidilute solutions.[42] Such a scaling has been also observed experimentally in linear viscoelasticity[43] studies of very similar systems.

The last case to be examined are the T2D blends, where the calculation of the N_e and ν_{PI} parameters is closely related to the question whether the diblock molecules participate in entanglements with the PI middle blocks of the SIS chains. Having in mind a picture of the PI block of a diblock being attached through its styrene block to a rigid PS-rich domain, while the isoprene end is dangling free in the PI-rich matrix, the analogy with an arm of a starlike polymer is obvious. In this context, an estimation of the disentanglement time of the PI parts of the diblocks in SBC materials can be attempted by invoking the results of Pearson and Helfand[44] for the arm relaxation time, τ_m, of starlike polymers. The original Pearson and Helfand result is reproduced below in an equivalent form, omitting prefactors[45] of the order of π:

$$\tau_m = \frac{N_a^{3/2}\zeta b^2\sqrt{N_e}}{k_B T}\exp(0.6N_a/N_e) \quad (24)$$

The parameter b stands for the Kuhn segment length, and N_a denotes the number of Kuhn segments in one "arm" of the star, while N_e is the chain contour length between two entanglements, also measured in Kuhn segments. We have additionally assumed that the friction coefficient of an N_a segment long polymer chain, $\bar{\zeta}$, is expressed through the friction coefficient of one Kuhn segment, ζ, as $\bar{\zeta} = N_a\zeta$. In our case, using data[46] for the self-diffusion coefficient D in the Rouse regime, it was possible to estimate ζ from the relationship $\zeta = k_B T/(N_a D)$ as $\zeta = 0.81 \times 10^{-10}$ N s/m. Following Helfand's interpretation of "Kuhn segments", the order of magnitude of b is 1 nm, so the relaxation time for the PI block in the SI chains is estimated to be around $\tau_m \sim 150$ s.

This result for τ_m is subject to considerable uncertainty due to the omitted numerical prefactors in eq 24. Nevertheless, we believe it to be a good approximate indicator of the characteristic time of the diblock disentanglement process in the T2D blends. The tensile experiments, carried out at rates of 500 mm/min on 15 mm high specimens, are faster than, or at least of the order of magnitude of, the disentanglement process. Actually, for an initial specimen height of 15 mm, the characteristic disentanglement time at a strain rate of 500 mm/min corresponds to a strain $\epsilon = 83$. Therefore, for the purpose of comparing against the experimental tensile measurements, it can be assumed that entanglements contributed by the polyisoprene blocks of the diblocks are "permanent" during the deformation process; the entanglement molecular weight for the triblock middle, PI, block will not be affected by the diblock presence and will equal the bulk MW_e(PI) value.

Having this point in mind and still considering the PI blocks of the triblocks as the load-bearing chains, the expression for G_e in the case of TD systems becomes

$$G_e = RT\,\frac{N_{SIS}}{N_e}(1 - f_{SIS})\nu_{PI}(SIS) = \frac{RT\rho_{0I}^{true}\beta_{SIS}(1 - \alpha_{SIS})}{MW_e(PI)[\beta_{SIS}(1 - \alpha_{SIS}) + (1 - \beta_{SIS})(1 - \alpha_{SI})]} \quad (25)$$

where ν_{PI}(SIS) is the number density of the PI blocks belonging to the SIS chains.

After the evaluation of the G_e, the parameter G_c can be rather trivially obtained from the first of eq 16, equivalent to eq 19 for networks with high functionality. (This is justified in our case since, for most systems in this work, more than 100 bridging chains emanate from a single polystyrene domain, i.e., $\varphi_{network} \geq 100$.)

The results obtained for G_e using the "forward" approach outlined above are presented in Table 6. The stress−strain curves obtained from eq 18 for the G_c and G_e estimated through the "forward" approach are shown at the top of Figure 9, where the tensile experiment data are also reproduced. It can be seen that for small strains ($\epsilon < 1.5$) the qualitative agreement between the theoretical prediction and the experimental observations is astonishingly good since the theory manages to grasp both the correct order of magnitude and the effect of diblock and resin content on the *relative* position of the corresponding stress−strain diagrams. However, one should point out that this agreement validates our estimation of the entanglement contribution more than our predictions of microphase separated morphologies and physical cross-linking between the polystyrene domains. This can be appreciated if one considers that, according to the data of Table 6, the G_e modulus is 2 or 3 orders of magnitude larger than the G_c modulus. Combining this with the fact that the stress−strain relationship of eq 18 for small values of ϵ becomes $\sigma(\epsilon) \approx 3(G_c + G_e)\,\epsilon$, the dominant role of entanglements in determining the elastic properties of SBC materials studied here at low strains becomes obvious.

In Table 6, we also present the results for G_c and G_e obtained through the regressive approach by fitting the tensile experiment data with the slip-tube model. These fits were good for the intermediate strain regime, i.e., for $1 < \epsilon < 3$, and are reproduced at the bottom of Figure 9. By comparing them with the tensile experimental curves, also shown on the same graph, it can be seen that the model cannot fit the hardening at large strains, which is due to the finite extensibility of the chains, but illustrates well the softening due to the release of the portion of the stress carried by nonpermanent topological constraints.

Figure 9 shows that it is possible through the "regressive" approach to obtain a parametrization of the slip-tube model rubber elasticity theory providing a better

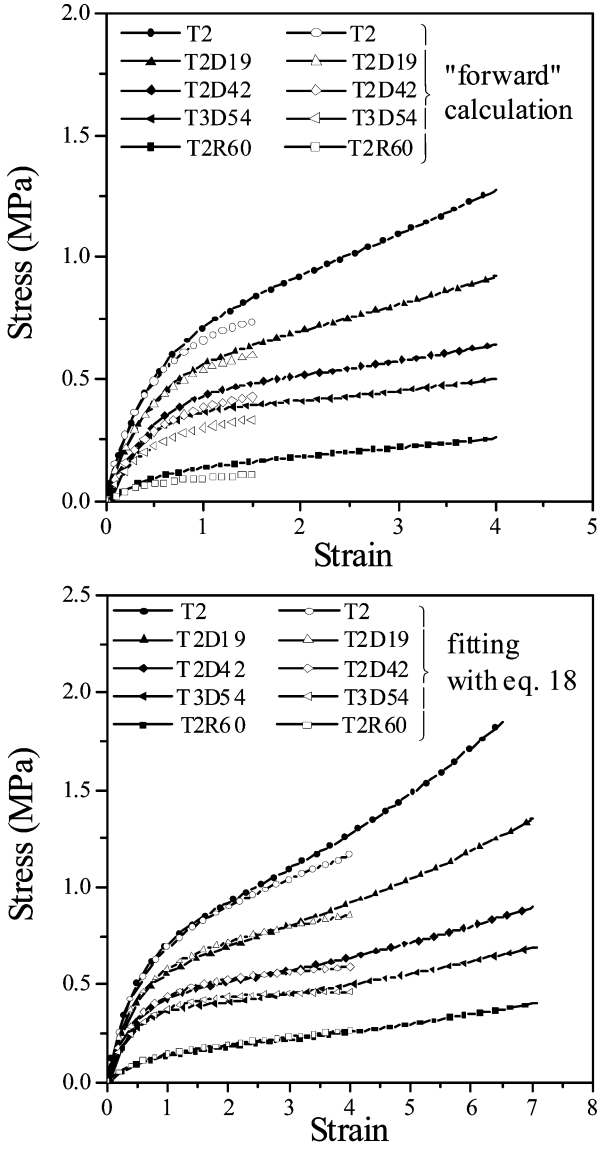

Figure 9. At the top are shown the nominal stress−strain curves for pure T2, T2D, and T3D blends and T2R60 solution, as measured experimentally (solid symbols) at a deformation rate of 500 mm min^{-1} and as calculated through the "forward" approach (open symbols) by combining SCF results with the slip-tube model rubber elasticity theory. At the bottom are shown the stress−strain curves (open symbols) obtained through a phenomenological "regressive" approach by fitting the experimentally obtained tensile curves (solid symbols) with the slip-tube model rubber elasticity theory.

description of the experimental data than the "forward" calculation based on molecular properties. In particular, the "forward" approach underestimates the G_c modulus, as a result of which the forward-calculated stress−strain curve becomes considerably flatter (i.e., corresponding to a "softer" material) at large strains than the fitted curve. The "forward" calculation underestimates the G_c modulus systematically in comparison to the "regressive" approach, the only exception being the T3D54 blend. On the contrary, the G_e modulus is overestimated by the "forward" approach in comparison to the regressive approach, with few exceptions (T2D42 and T3D54 blends). One reason for these differences could be that the "forward" calculations have been conducted on perfectly ordered nanophase separated structures (bcc arrangement). On the contrary, as was discussed in section 6.1, the real SBC materials are characterized by a rather random, "liquidlike" arrangement of the PS micelles. In addition, it should be taken into account that the "forward" calculation of G_c and G_e is a *thermodynamic calculation* and is not considering any rate-dependent energy dissipation process during the deformation of these materials.

7. Concluding Remarks

We have successfully used SCF theory to predict the morphology of three-component microphase separated block copolymer self-adhesive materials as well as the volume density of bridges between hard spherical domains. Concerning the morphology, our simulations are in quantitative agreement with the results obtained by SAXS and AFM of the microphase separated structure. Although the experimentally characterized structures show less long-range order than the fully equilibrated structures in the simulations, the main characteristic distances (interparticle distance and radius of the PS domains) are well predicted by the simulations. The discrepancy could well be due to the annealing conditions of the samples, which are not expected to lead to fully equilibrated structures. When calculations on larger boxes were performed, the model system became trapped in metastable states which were invariant with box size and reproduced the experimental observations very closely.

The volume fraction of resin molecules in each of the two phases (a piece of information which cannot be easily obtained by experiments) can be predicted by the simulation. This type of information will be particularly useful when attempting to predict the range of service temperatures of a particular adhesive blend.

Finally, SCF simulations have proved to be a powerful tool to investigate not only the structure of phase separated block copolymer blends but also the connectivity between domains, which has a profound influence on the nonlinear elastic properties of the blends and ultimately on the fracture and adhesive properties of the material. We expect that such a tool will prove particularly useful when more complicated block copolymer architectures will be tested as base polymers for these blends.

A possible improvement to the model could be the consideration, during the elasticity modulus calculations, of imperfectly formed microphase-separated structures, representative of the real experimental situation. A deeper insight into the mechanical properties of SBC can be obtained, however, through integrating the SCF 3D real-space calculations with mesoscopic simulations of the actual deformation process, such as the network-based kinetic Monte Carlo strategy of Terzis et al.,[18−20] which explicitly accounts for the entanglements present in the polymeric system.

Acknowledgment. We are indebted to Dr. Raymond Ober at the Collège de France for his help in obtaining the X-ray data and to Dr. Christian Frétigny for his help with the AFM experiments. We are grateful to Dr. V. A. Harmandaris for his contribution to the development of SCF software. We thank Dr. V. G. Mavrantzas and Dr. A. F. Terzis for many helpful discussions. This work was supported by the European Commission through a GROWTH project, Contract G5RD-CT 2000-00202 (DEFSAM).

Appendix. Evaluation of Parameters for the Mesoscopic Representation of SBC's

To accomplish the mesoscopic description of SBC's, it is necessary to specify the quantities f_{SIS}, f_{SI}, $\chi_{SI}\langle N\rangle$, $\chi_{SR}\langle N\rangle$, $\chi_{IR}\langle N\rangle$, $N_{SIS}/\langle N\rangle$, $N_{SI}/\langle N\rangle$, and $1/\langle N\rangle$, the evaluation of which is closely related to the invariance of the characteristic macroscopic volumes. This can be appreciated, for example, in the most general case of SIS/SI/resin mixtures by integrating the equations relating the volume fractions to the propagators q and q^+ (eq 8). In this way we obtain

$$\frac{\int \phi_S(\mathbf{r})\,d\mathbf{r}}{V} = \frac{\tilde{n}_{SIS}N_{SIS}2f_{SIS}}{\langle N\rangle} + \frac{\tilde{n}_{SI}N_{SI}f_{SI}}{\langle N\rangle}$$

$$\frac{\int \phi_I(\mathbf{r})\,d\mathbf{r}}{V} = \frac{\tilde{n}_{SIS}N_{SIS}(1-2f_{SIS})}{\langle N\rangle} + \frac{\tilde{n}_{SI}N_{SI}(1-f_{SI})}{\langle N\rangle}$$

$$\frac{\int \phi_R(\mathbf{r})\,d\mathbf{r}}{V} = \frac{\tilde{n}_R}{\langle N\rangle} \qquad \text{(A.1)}$$

Because of the invariance of volume fractions, the left-hand-side integrals are evaluated as

$$\frac{\int \phi_S(\mathbf{r})\,d\mathbf{r}}{V} = \frac{\int \rho_S^{true}(\mathbf{r})\,d\mathbf{r}}{V\rho_{S0}^{true}} = \frac{V_S}{V},$$

$$\frac{\int \phi_I(\mathbf{r})\,d\mathbf{r}}{V} = \frac{\int \rho_I^{true}(\mathbf{r})\,d\mathbf{r}}{V\rho_{I0}^{true}} = \frac{V_I}{V} \qquad \text{(A.2)}$$

The superscript "true" in the above equations shows that the number density refers to real system "microscopic" number density. Since volumes V_{SIS}^S, V_{SIS}^I, V_{SI}^S, V_{SI}^I, and V_R are also considered as invariants, following the same method it can be shown that

$$\frac{V_{SIS}^S}{V} = \frac{\tilde{n}_{SIS}N_{SIS}2f_{SIS}}{\langle N\rangle}, \quad \frac{V_{SI}^S}{V} = \frac{\tilde{n}_{SI}N_{SI}f_{SI}}{\langle N\rangle},$$

$$\frac{V_{SIS}^I}{V} = \frac{\tilde{n}_{SIS}N_{SIS}(1-2f_{SIS})}{\langle N\rangle}, \quad \frac{V_{SI}^I}{V} = \frac{\tilde{n}_{SI}N_{SI}(1-f_{SI})}{\langle N\rangle},$$

$$\frac{V_R}{V} = \frac{\tilde{n}_R}{\langle N\rangle} \qquad \text{(A.3)}$$

where the ratio $1/\langle N\rangle$ is defined in terms of total system volume, resin volume, and resin molar fraction, which are invariants. Simple manipulations of eqs A.3 lead to the following expressions for the parameters f_{SIS}, f_{SI}, $N_{SIS}/\langle N\rangle$, and $N_{SI}/\langle N\rangle$:

$$\frac{V_{SIS}^S}{V_{SIS}^I} = \frac{2f_{SIS}}{(1-2f_{SIS})}, \quad \frac{V_{SI}^S}{V_{SI}^I} = \frac{f_{SI}}{(1-f_{SI})},$$

$$\frac{V_{SIS}^S + V_{SIS}^I}{\tilde{n}_{SIS}V} = \frac{N_{SIS}}{\langle N\rangle}, \quad \frac{V_{SI}^S + V_{SI}^I}{\tilde{n}_{SI}V} = \frac{N_{SI}}{\langle N\rangle} \qquad \text{(A.4)}$$

The appearance of macroscopic volumes in the above equations in the form of ratios is very convenient for the evaluation of the parameters, since any arbitrary quantity of the mixture can be considered. Taking for example 1 g of SIS/SI/resin mixture, given the weight fraction of styrene in the SIS and SI molecules (denoted by α_{SIS} and α_{SI}, respectively) as well as the total composition of the copolymer/resin mixture defined by the weight fractions of SI, SIS, and resin (denoted by β_{SI}, β_{SIS}, and $\beta_R = 1 - \beta_{SI} - \beta_{SIS}$), with $\tilde{\rho}_{S0}^{true}$ and $\tilde{\rho}_{I0}^{true}$ denoting the true mass densities of polystyrene and polyisoprene, respectively, the characteristic macroscopic volumes are

$$V_{SI}^S = \frac{\beta_{SI}\alpha_{SI}}{\tilde{\rho}_{S0}^{true}}, \quad V_{SI}^I = \frac{\beta_{SI}(1-\alpha_{SI})}{\tilde{\rho}_{I0}^{true}}, \quad V_{SIS}^S = \frac{\beta_{SIS}\alpha_{SIS}}{\tilde{\rho}_{S0}^{true}},$$

$$V_{SIS}^I = \frac{\beta_{SIS}(1-\alpha_{SIS})}{\tilde{\rho}_{I0}^{true}}, \quad V_R = \frac{(1-\beta_{SI}-\beta_{SIS})}{\tilde{\rho}_{R0}^{true}},$$

$$V = V_{SI}^S + V_{SI}^I + V_{SIS}^S + V_{SIS}^I + V_R \qquad \text{(A.5)}$$

These volumes can be substituted into eqs A.4 along with the molar fractions, giving the final results for the parameters f_{SIS}, f_{SI}, $N_{SIS}/\langle N\rangle$, and $N_{SI}/\langle N\rangle$.

The last set of quantities to be established are the products $\chi_{SI}\langle N\rangle$, $\chi_{SR}\langle N\rangle$, and $\chi_{IR}\langle N\rangle$, which can be easily expressed in terms of invariants as follows:

$$\chi_{AB}\langle N\rangle = \chi_{AB}\rho_0\frac{\langle N\rangle}{\rho_0} = \chi_{AB}\rho_0\frac{\langle N\rangle V}{n_{SIS}N_{SIS} + n_{SI}N_{SI} + n_R} = \chi_{AB}\rho_0\frac{V}{n_{SIS} + n_{SI} + n_R} \qquad \text{(A.6)}$$

References and Notes

(1) Satas, D., Ed. *Handbook of Pressure Sensitive Adhesive Technology*; Van Nostrand Reinhold: New York, 1989.
(2) Creton, C. *MRS Bull.* **2003**, *28*, 434.
(3) Nakajima, N.; Babrowicz, R.; Harrell, E. R. *J. Polym. Sci., Polym. Phys. Ed.* **1992**, *44*, 1437.
(4) Kraus, G.; Rollmann, K. W.; Gray, R. A. *J. Adhes.* **1979**, *10*, 221.
(5) Brown, K.; Hooker, J. C.; Creton, C. *Macromol. Mater. Eng.* **2002**, *287*, 163.
(6) Helfand, E. *J. Chem. Phys.* **1975**, *62*, 999.
(7) Helfand, E. *Macromolecules* **1975**, *8*, 552.
(8) Helfand, E.; Sapse, A. *J. Chem. Phys.* **1975**, *62*, 1327.
(9) Helfand, E.; Wasserman, Z. R. *Macromolecules* **1976**, *9*, 879.
(10) Helfand, E.; Wasserman, Z. R. *Macromolecules* **1978**, *11*, 960.
(11) Matsen, M. W.; Schick, M. *Phys. Rev. Lett.* **1994**, *72*, 2660.
(12) Drolet, F.; Fredrickson, G. H. *Phys. Rev. Lett.* **1999**, *83*, 4317.
(13) Fraaije, J. G. E. M. *J. Chem. Phys.* **1993**, *99*, 9202.
(14) Fredrickson, G. H.; Ganesan, V.; Drolet, F. *Macromolecules* **2002**, *35*, 16.
(15) Drolet, F.; Fredrickson, G. H. *Macromolecules* **2001**, *34*, 5317.
(16) Altevogt, P.; Evers, O. A.; Fraaije, J. G. E. M.; Maurits, N. M.; van Vlimmeren, B. A. C. *THEOCHEM* **1999**, *463*, 139.
(17) OCTA simulation package, Nagoya University, http://octa.jp.
(18) Terzis, A. F.; Theodorou, D. N.; Stroeks, A. *Macromolecules* **2000**, *33*, 1385.
(19) Terzis, A. F.; Theodorou, D. N.; Stroeks, A. *Macromolecules* **2000**, *33*, 1397.
(20) Terzis, A. F.; Theodorou, D. N.; Stroeks, A. *Macromolecules* **2002**, *35*, 508.
(21) Rubinstein, M.; Panyukov, S. *Macromolecules* **2002**, *35*, 6670.
(22) Roos, A.; Creton, C., to be published.
(23) Helfand, E.; Tagami, Y. *J. Chem. Phys.* **1972**, 3592.
(24) Fischel, L. B.; Theodorou, D. N. *J. Chem. Soc., Faraday Trans.* **1995**, *91*, 2381.
(25) Scheutjens, J. M. H. M.; Fleer, G. J. *J. Chem. Phys.* **1979**, *83*, 1619.
(26) Takahashi, K.; Yunoki, Y. *J. Phys. Soc. Jpn.* **1967**, *22*, 219.
(27) Morse, D. C.; Fredrickson, G. H. *Phys. Rev. Lett.* **1994**, *73*, 3235.
(28) Matsen, M. W. *J. Chem. Phys.* **1996**, *104*, 7758.
(29) Schmid, F. *J. Phys*: *Condens. Matter* **1998**, *10*, 8105.
(30) Hashimoto, T.; Shibayama, M.; Kawai, H. *Macromolecules* **1980**, *13*, 1237.
(31) Matsen, M. W.; Bates, F. S. *Macromolecules* **1996**, *29*, 1091.
(32) Hong, K. M.; Noolandi, J. *Macromolecules* **1981**, *14*, 727.

(33) Matsen, M. W.; Thompson, R. B. *J. Chem. Phys.* **1999**, *111*, 7139.
(34) Mark, J. E. *Physical Properties of Polymers Handbook*; American Institute of Physics: Woodbury, NY, 1996.
(35) Han, C. D.; Kim, J. *Macromolecules* **1989**, *22*, 382.
(36) Higgins, J. S.; Benoit, H. C. *Polymers and Neutron Scattering*; Clarendon Press: Oxford, 1996.
(37) Morita H.; Kawakatsu, T.; Doi, M.; Yamaguchi, D.; Takenaka, M.; Hashimoto, T. *Macromolecules* **2002**, *35*, 7473.
(38) Choi, S.; Lee, K. M.; Han, C. D.; Sota, N.; Hashimoto, T. *Macromolecules* **2003**, *36*, 793.
(39) Laurer, J. H.; Bukovnik, R.; Spontak, R. J. *Macromolecules* **1996**, *29*, 5762.
(40) Hadziioannou, G.; Skoulios, A. *Macromolecules* **1982**, *15*, 267.
(41) Hashimoto, T.; Fujimura, M.; Kawai, H. *Macromolecules* **1980**, *13*, 1660.
(42) de Gennes, P. G. *Macromolecules* **1976**, *9*, 587.
(43) Gibert, F. X.; Marin, G.; Derail, C.; Allal, A.; Lechat, J. *J. Adhes.* **2003**, *79*, 825. Gibert, F. X. Ph.D. Thesis, Université de Pau et Pays de l'Adour, 2001.
(44) Pearson, D. S.; Helfand, E. *Macromolecules* **1984**, *17*, 888.
(45) Klein, J. *Macromolecules* **1986**, *19*, 105.
(46) Doxastakis, M. Ph.D. Thesis, University of Patras, 2001.

MA035383A